Shock Compressing Diamond to a Conducting Fluid

D. K Bradley, J. H. Eggert, D. G. Hicks, P. M. Celliers, S. J. Moon, R. C. Cauble, and G. W. Collins

Lawrence Livermore National Laboratory, Livermore, California 94551, USA

(Received 7 April 2004; published 5 November 2004)

Laser generated shock reflectance data show that diamond undergoes a continuous transition from optically absorbing to reflecting between Hugoniot pressures $600 < P_H < 1000$ GPa. The data are consistent with diamond having a thermal population of carriers at $P_H \sim 600$ GPa, undergoing band overlap metallization at $P_H \sim 1000$ GPa and melting at $800 < P_H < 1000$ GPa. The results agree well with an equation of state model that predicts that elemental carbon remains solid throughout the interior of Neptune.

DOI: 10.1103/PhysRevLett.93.195506 PACS numbers: 62.50.+p, 64.70.Dv, 71.30.+h

Carbon is a basic building block of life, a primary constituent of Uranus, Neptune [1], and white dwarfs and is used in many technological applications. The unique properties of the diamond phase, including its extreme hardness and low compressibility, have made possible static high-pressure research up to several hundred GPa [2]. However, the properties of diamond at higher pressures remain unknown [3–13]. We report on measurements that show that diamond melts to a conducting fluid between 600 and 1000 GPa on the principal Hugoniot. At pressures just below the onset of melt, our analysis suggests that the band gap closes. These observations suggest that pure carbon in the deep interior of Neptune would be in an insulating solid phase.

The multiple hybridizations of carbon's valence electrons result in a complicated phase diagram. Although the region around the graphite-liquid melt line has been studied extensively by several authors [14–16] (showing that liquid carbon, at temperatures just above the melt line is a semimetal), experimental data in the high-pressure region around the diamond melt curve are sparse [4]. Figure 1 shows one high-pressure phase diagram, proposed by van Thiel and Ree [12] (VTR). Superimposed on the VTR diagram are several theoretical diamond Hugoniots and melting curves [8,11,13,17] and an isentrope that lies close to predicted core conditions of Neptune [18]. As can be seen, for all but the VTR model the high-pressure part of the isentrope is predicted to lie in the molten phase. In addition to the melting transition, several authors [7,8,19] predict that diamond will transform to a metallic BC8 phase before melting. This predicted insulating to metallic-solid transition is incorporated into the phase diagram proposed by Kerley and Chhabildas (KC) [8] and accounts for the changes in slope along the KC Hugoniot (Fig. 1) at 430–500 GPa.

Experiments were conducted using the 351 nm OMEGA laser system at the University of Rochester. Targets consisted of 100 or 500 μm thick natural type 2a diamond flats oriented along the (110) axis and glued onto the thin side of an Al step. A low-Z plastic (CH) ablator on the drive side of the Al pusher reduced the quantity of high energy x rays produced at the ablation front that can preheat the target. A thin (100 nm) coating of Al on the laser-drive side of the CH ensured that the laser plasma originated away from the Al plate [20]. The diamond surface was coated with an Al_2O_3 antireflection coating to minimize reflection of the probe beam. A typical target is shown in Fig. 2. The drive laser produces a shock, which propagates through the pusher and into the diamond sample. Steady shocks were achieved with 3.5 ns

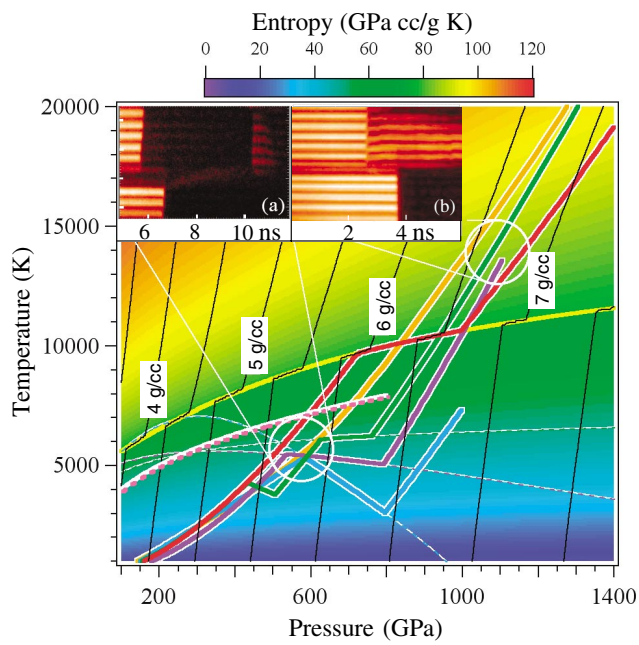

FIG. 1 (color). Temperature versus pressure phase diagram for diamond together with the melt (yellow line), Hugoniot (red line), constant densities (black lines), and entropy (color shading) as calculated by VTR [12]. Other Hugoniot predictions include Kerley and Chhabildas (KC) [8] (green line), Molodets [13] (purple line), Fried [11] (blue line), and Sesame [17] (orange line). The pink dashed line is a calculated isentrope of Neptune [18]. The inset VISAR (velocity interferometer system for any reflector) images are from diamond shock compressed to (a) 550–600 GPa and (b) 1100 GPa and are discussed in the text. The graphite phase of carbon lies to lower temperatures and pressures than those shown in the figure.

 © 2004 The American Physical Society

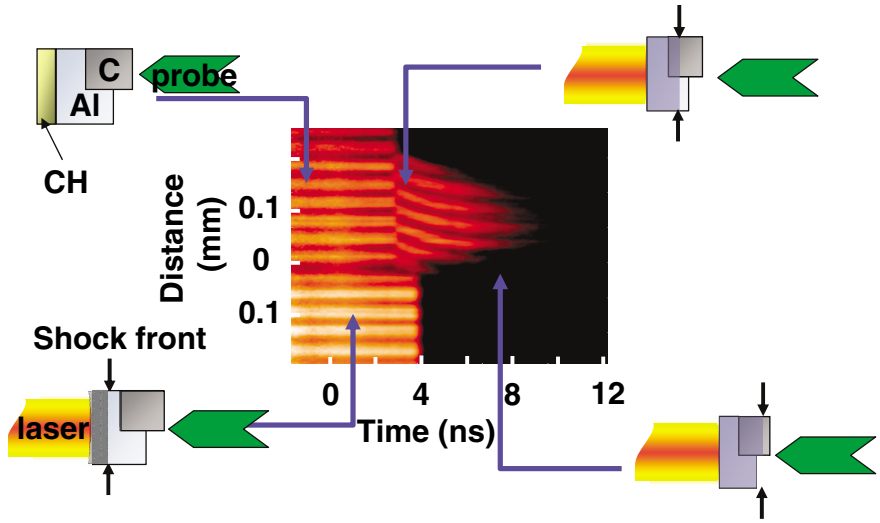

FIG. 2 (color). Typical target and VISAR image for decaying shock used to measure shock reflectance versus shock velocity over the transition region between reflective and nonreflective states. Time zero on this image is set to the beginning of the drive pulse. (i) Before the start of laser-drive pulse, unshifted fringes are seen. (ii) After the start of drive, fringes are still unshifted as shock has not reached rear surface. (iii) The shock has broken out into diamond. Shifted fringes are reflected from the shock front in diamond. Unshifted fringes are still seen from the thick Al step. (iv) The shock has broken out from the thick Al step.

flat-top pulse shapes. Decaying shocks, used for mapping shock reflectance over a continuous pressure range, were produced with 1 ns flat-top pulse shapes. Shock planarity (2% over 300 μm upon breakout from a 50 μm Al target) was achieved using continuous phase plates having a flat-top footprint of 650 μm.

A line VISAR diagnostic [21] operating at 532 nm measured the shock velocity in diamond U_s^{diamond} versus time by detecting the Doppler shift of light reflecting off the shock front [22]. Laser light reflected from the target is imaged through an interferometer onto the slit of an optical streak camera. The resulting streaked image contains a series of fringes, whose phase is directly proportional to the velocity of the reflecting surface [23].

In general, transparent materials undergo a series of similar optical responses, from transparent, to nontransparent (due to absorption or diffusive scattering), to reflecting with increasing shock pressure. At low pressures ($\leq$100 GPa) shocked diamond is known to be transparent [24] (reflecting surfaces can be observed with a VISAR through a shocked diamond window), and we have used it as a window material for 1064 nm light for shocks up to 120 GPa. At $\sim 300 < P < 600$ GPa, shocked diamond is nontransparent (the reflected intensity at the VISAR detector lacks any contribution from surfaces beyond the shock front) and any VISAR signal at 532 nm ($R_{\lambda=532\,\mathrm{nm}}$) from a potentially reflecting shock is below our detection limit of 0.1%–1%. An example VISAR record for $P =$ 550–600 GPa (as determined by simulation and average transit time through the diamond) is shown in Fig. 1 [inset (a)]. Following the VISAR fringes in time (from left to right) we note that before the shock breaks out from the Al, steady unshifted fringes are seen. Since no fringe shift is detected until the shock wave reaches the surface of the thin Al step and breaks out into the diamond, we estimate the preheat in the Al to be below 600 K. At $\sim$5.5 ns the shock breaks out into the diamond and the reflected signal drops to near our detection limit. At $\sim$6.5 ns the shock breaks out of the thick Al step, and the reflection from the Al surface rapidly vanishes. The loss of surface reflectivity is due to the rapid development of a density gradient when a surface without strength (fluid) unloads into vacuum [25]. At $\sim$10 ns the shock front breaks out from the rear surface of the diamond and in this case a bright series of fringes (10%–20% reflective) return. This fringe recovery occurs when a material with strength (solid) unloads into a vacuum (the antireflection coating on a window is generally destroyed by a strong shock).

The VISAR image in Fig. 1(b) [inset (b)] is from diamond shocked to a high pressure of $\sim$1050 GPa, which is above the predicted melt pressure P_{melt} for all the models. Strong fringes are seen when the shock breaks out from the thin Al step into the diamond at 2.4 ns. The discontinuity seen at this time is caused by the streak camera being unable to resolve the rapid change in phase ($\sim$4 fringes) as the VISAR probe starts to reflect off the rapidly moving shock front. The shock velocity in the diamond (confirmed by a second VISAR with a different sensitivity) ranged from 25 μm/ns just after breakout to 26.4 μm/ns after 3 ns. The reflectivity from the shock, $R_{\lambda=532\,\mathrm{nm}} \sim 30\%$, was calculated by comparing to the reflectivity of the thicker (bare) Al step, which was taken to be 85% [26]. This value for $R_{\lambda=532\,\mathrm{nm}}$ in diamond is more than an order of magnitude higher than expected from a Fresnel reflection and, as is discussed below, results from reflection off a conducting phase of carbon.

In order to probe the transition region between nonreflecting (nonconducting) and reflecting (conducting) phases, a temporally short (1 ns) laser pulse was used to launch a shock that decays with time continuously over a large pressure range. This technique allows a large pressure range to be sampled on a single shot and minimizes random uncertainties in reflectance at different pressures. While the shot to shot uncertainty in reflectance can be as high as 30%, the relative uncertainty within a single shot

is much less. Figure 2 shows an experimental VISAR data record which spans from $P \sim 1500$ GPa just after shock breakout into the diamond to ~500 GPa near the end of the data record. After the shock enters the diamond, the normalized reflected probe intensity is at a high value and then decays to the background level. This observation is analyzed to give a continuous record of $R_{\lambda=532\,\mathrm{nm}}$ from shock compressed diamond and U_s^{diamond} from the fringe phase shift. While the shock front pressure decreases with time, the shock front is always on the Hugoniot. Although there is a P-ρ-T gradient behind the shock front, over an optical depth (~40 nm) the variations in P-ρ-T are very small.

Figure 3 shows $R_{\lambda=532\,\mathrm{nm}}$ plotted versus U_s^{diamond} for two shots. The shock front reflectance is constant at about 30% over a wide range of shock velocities above 24.5 μm/ns ($P > 1000$ GPa). As U_s^{diamond} drops from 24.5 to 20.2 μm/ns (1000 to 600 GPa), $R_{\lambda=532\,\mathrm{nm}}$ falls from 30% to 0.1% which is the detection limit. The measured insulating-conducting transition region is a little larger than but very close to the predicted solid-liquid coexistence region in VTR ($22.0 < U_s < 24.6$ μm/ns). There is a strong correlation between the increase in $R_{\lambda=532\,\mathrm{nm}}$ and the calculated liquid fraction from VTR as shown by the blue curve in Fig. 3. Additional evidence for a melting transition is found by studying the release of the shock from the rear surface of the diamond. As seen in Fig. 1, for shocks below the conducting transition ($U_s < 20\mu$m/ns or about 550 GPa), we see reflective fringes as the shock exits the free surface. The presence of fringes after shock breakout indicates reflection off a solid surface with strength. In contrast for the higher-pressure shocks, where the diamond shock front is reflective ($U_s > 25\mu$m/ns or about 1000 GPa), the reflectance abruptly falls to zero upon shock breakout from the diamond-vacuum interface. This behavior is consistent with free-surface unloading of a high-pressure fluid. The unloading fluid rapidly develops a density gradient of several tenths of a micron, which is sufficient to extinguish the reflected probe signal [27]. This observation is strongly indicative of a solid-liquid phase transition occurring in the vicinity of the optical transition.

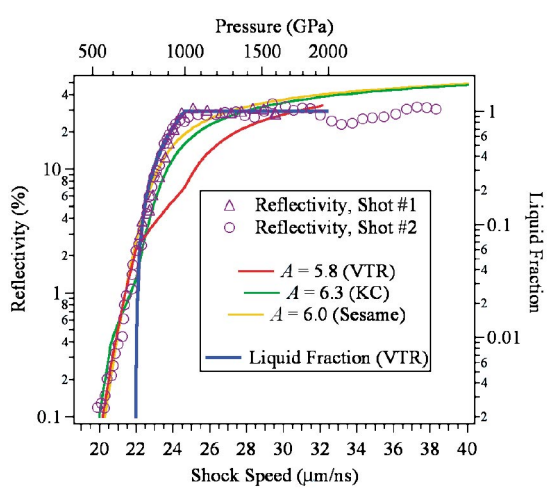

FIG. 3 (color). Measured shock reflectance versus shock velocity. The shock pressure axis is calculated from the shock velocity using the VTR EOS [12], which is limited to pressures below 2000 GPa. The solid lines are fits to the Sommerfeld model described in the text using $\gamma = 4$, $\tau = \tau_{\min}$, and $m = m_e$. The solid lines shown use the following EOS and values for A: red line—VTR [12], $A = 5.8$ eV; green line—KC [8] $A = 6.3$ eV; orange line—Sesame [17], $A = 6.0$ eV. The blue dotted line is the liquid volume fraction using the VTR equation of state (EOS).

While the sharp saturation in reflectivity seen in our data at 24.5 μm/ns is consistent with melting to a conducting state, the exponential increase in reflectance with velocity at lower pressure cannot be ascribed entirely to melting. Shock reflectance measurements in LiF, Al_2O_3 [28], and water [29] have been well matched using a semiconducting (Sommerfeld) model with a small band gap and a scattering time that meets the Ioffe-Regel criterion [30]. This model assumes that the rise in reflectance is due to thermal excitation of electrons across a mobility gap.

We have modeled our reflectance data using a similar model. Reflectivity is calculated using the Fresnel equations, $R = |(\sqrt{\varepsilon} - n_d)/(\sqrt{\varepsilon} + n_d)|^2$, where $n_d = 2.424$ is the refractive index of the unshocked diamond. The complex dielectric constant of the shocked material ε is calculated from a Drüde formulation such that $\varepsilon = (\varepsilon_b - \frac{\omega_p^2}{\omega^2(1+i/\omega\tau)})$, where $\varepsilon_b = n_d^2$ represents the bound electron contribution and is assumed to be constant, $\omega_p^2 = \frac{n_e e^2}{\varepsilon_0 m_e}$ is the plasma frequency, and τ is the electron scattering time, which for this analysis is assumed to be equal to the Ioffe-Regel minimum scattering time. The scattering time is expressed as $\tau = \tau_{\min} = \frac{2}{v_e}(\frac{3}{4\pi n_{\mathrm{atom}}})^{1/3}$, where n_{atom} is the atomic density, and v_e is the average carrier velocity, which is calculated by integrating over the Fermi distribution at a given temperature. The electron number density $n_e = \gamma \int g_c(E) f(E,T) dE$, where γ is the electron degeneracy, g_c is the electronic density of states, and f is the Fermi-Dirac distribution function. The band gap, or mobility gap, of the semiconductor enters the analysis through the density of states.

In diamond the temperature at the onset of high shock reflectance is low enough (0.4–0.5 eV) for all EOS's considered that substantial thermal excitation of free carriers could occur only for a mobility gap far smaller than at ambient pressure. We have therefore modeled the diamond reflectance data using a density dependant mobility gap, $E_{\mathrm{gap}} = E_0 - A(\rho/\rho_0 - 1)$, where $E_0 = 5.45$ eV is the zero pressure band gap, A is a constant, ρ is the density, and ρ_0 is the zero pressure density [28]. This is consistent with several theoretical

predictions that have reported a reduction in E_{gap} with increasing deviatory stress [31–33]. Fits to our data using this model give $A = 6.01 \pm 0.50$ eV so that the mobility gap closes (metallization) at $U_s = 24.3 \pm 2.0$ μm/ns, $\rho = 6.7 \pm 0.3$ g/cc, $P = 1000 \pm 200$ GPa, and $T = 12\,000 \pm 4000$ K. The large uncertainty in temperature is dominated by the large disagreement in temperatures arising from various treatments of the melt transition by the different equations of state considered here. Fits for a selection of EOS models are shown in Fig. 3. It is clear that while the analysis matches the low reflectance data quite well, the saturation at about 30% is much sharper experimentally than can be reproduced solely with this model. Our conclusion is that the best match to the complete data set is provided by a model that combines both a semiconducting solid with a closing band gap and an eventual transition to a conducting fluid. The diamond-metallic (BC8) solid transition predicted by the KC EOS at 440–500 GPa lies below our observed absorbing to reflecting transition. We see no evidence of a conducting phase in the 300–500 GPa region, although it is possible that the time scale for this transition is slower than our experiment.

In summary, laser-driven shock wave experiments have been used to investigate the properties of diamond on its principal Hugoniot between 600 and 3000 GPa. Reflectivity measurements show that shock compressed diamond is opaque below 600 GPa, has shock reflectance which increases with pressure between 600 and 1000 GPa, and has nearly constant shock reflectance of about 30% above 1000 GPa. This increase in shock reflectance is caused by a transition to a metallic phase resulting from mobility-gap closure and shock-induced melting. Reflectance measurements of shock front unloading from the free surface are consistent with diamond being solid for $P < 550$ GPa and fluid for $P > 1000$ GPa. Our measured optical transition is strongly correlated with the solid-liquid coexistence region in the VTR EOS. If the melt transition predicted by VTR is correct, then the ice layers of Neptune and Uranus should contain carbon in the solid phase [6].

This work was performed under the auspices of the U.S. Department of Energy by University of California, Lawrence Livermore National Laboratory under Contract No. W-7405-Eng-48.

[1] W. B. Hubbard, Science **214**, 145 (1981).
[2] P. Loubeyre, F. Occelli, and R. LeToullec, Nature (London) **416**, 613 (2002).
[3] J.W. Shaner *et al.*, J. Phys. (Paris), Colloq. **45**, C8-235 (1984).
[4] F. P. Bundy *et al.*, Carbon **34**, 141 (1996).
[5] J. A. Van Vechten, Phys. Rev. B **7**, 1479 (1973).
[6] M. Ross, Nature (London) **292**, 435 (1981).
[7] R. Grover, J. Chem. Phys. **71**, 3824 (1979).
[8] G. I. Kerley and L. Chhabildas, Sandia National Laboratories Report No. SAND2001-2619, 2001.
[9] M. P. Grumbach and R. M. Martin, Phys. Rev. B **54**, R15 730 (1996).
[10] D. A. Young and R. Grover, in *Shock Waves in Condensed Matter 1987, Proceedings of the American Physical Society Topical Conference*, edited by S. C. Schmidt and N. C. Holmes (North-Holland, Amsterdam, 1988), pp. 131–134.
[11] L. E. Fried and W. M. Howard, Phys. Rev. B **61**, 8734 (2000).
[12] M. van Thiel and F. H. Ree, High Press. Res. **10**, 607 (1992).
[13] A. M. Molodets, M. A. Molodets, and S. S. Nabatov, in *Shock Compression of Condensed Matter*, edited by S. C. Schmidt, D. P. Dandekar, and J.W. Forbes (AIP Press, Melville, NY, 1998), Vol. 429, p. 91.
[14] F. P. Bundy, J. Chem. Phys. **38**, 618 (1963).
[15] N. S. Fateeva and L. F. Vereshchagin, Pis'ma Zh. Eksp. Teor. Fiz. **13**, 157 (1971).
[16] M. Togaya, Phys. Rev. Lett. **79**, 2474 (1997).
[17] S. P. Lyon and J. D. Johnson, Los Alamos National Laboratory Report No. LA-UR-92-3407, 1992.
[18] W. B. Hubbard, M. Podolak, and D. J. Stevenson, *Neptune and Triton* (University of Arizona Press, Tucson, AZ, 1995), p. 109.
[19] S. Fahy and S. G. Louie, Phys. Rev. B **36**, 3373 (1987).
[20] D. K. Bradley *et al.*, in *Laser Interaction and Related Plasma Phenomena*, edited by H. Hora and G. H. Miley (Plenum Press, New York, 1991), Vol. 7, p. 323.
[21] L. M. Barker and R. E. Hollenbach, J. Appl. Phys. **43**, 4669 (1972).
[22] P. M. Celliers *et al.*, Appl. Phys. Lett. **73**, 1320 (1998).
[23] P. M Celliers *et al.*, Rev. Sci. Instrum. (to be published).
[24] C. S. Yoo *et al.*, Phys. Rev. Lett. **70**, 3931 (1993).
[25] P. Celliers and A. Ng, Phys. Rev. E **47**, 3547 (1993).
[26] P. M. Celliers *et al.*, Phys. Rev. Lett. **84**, 5564 (2000).
[27] W. L. Kruer, *Physics of Laser Plasma Interactions* (Addison-Wesley, Redwood City, CA, 1988).
[28] D. G. Hicks *et al.*, Phys. Rev. Lett. **91**, 035502 (2003).
[29] P. M. Celliers *et al.*, Phys. Plasmas **11**, L41 (2004).
[30] S. B. Kormer, Sov. Phys. Usp. **11**, 229 (1968).
[31] M. P. Surh, S. G. Louie, and M. L. Cohen, Phys. Rev. B **45**, 8239 (1992).
[32] H. K. Mao and R. J. Hemley, Nature (London) **351**, 721 (1991).
[33] O. H. Nielsen, Phys. Rev. B **34**, 5808 (1986).